

Resistivity model in both paramagnetic and ferromagnetic phases

Andrew Das Arulsamy¹

¹*Condensed Matter Group, Division of Exotic Matter, No. 22,
Jalan Melur 14, Taman Melur, 68000 Ampang, Selangor DE, Malaysia*

(Dated: March 22, 2022)

The resistivity model as a function of temperature and ionization energy (doping) is derived with further confinements from spin-disorder scattering in ferromagnetic phase. Magnetization and polaronic effects capture the mechanism of both spin independent and spin-assisted charge transport of ferromagnets. The computed $T_{crossover}$ below T_C and carrier density in $\text{Ga}_{1-x}\text{Mn}_x\text{As}$ system are 8-12 K and 10^{19} cm^{-3} , remarkably identical with the experimental values of 10-12 K and $10^{18-10^{20}} \text{ cm}^{-3}$ respectively.

PACS numbers: 72.10.Bg; 71.30.+h; 71.38.Ht; 75.50.Pp

Keywords: Ferromagnets, Resistivity model, Ionization energy, Fermi-Dirac statistics

1. INTRODUCTION

Diluted magnetic semiconductors (DMS) have the tremendous potential for the development of spintronics and subsequently will lay the foundation to realize quantum computing. This applicability arises due to ferromagnetic nature of DMS. In other words, both the charge and spin of the electrons can be exploited with limited Mn doping in GaAs semiconductor. In order to achieve this, one needs to understand the transport mechanism such as the variation of resistivity with temperature and doping in both above and below T_C consistently. Interestingly, Van Esch *et al.* [1] have proposed multiple exchange interactions, which are ferromagnetic (FM) hole-hole and antiferromagnetic (AFM) Mn-hole interactions for DMS. These two effects, after neglecting the direct exchange between Mn-Mn (due to very diluted nature of DMS) are seem to be sufficient enough to describe the temperature dependent magnetization curves ($M(T)$) accurately. However, even after inclusion of FM and AFM effects including the spin disorder scattering, the transport property in the FM phase is still not well understood. Unfortunately, this is also true for the case of metallic property below T_C in the well known and extensively studied FM manganites as pointed out by Mahendiran *et al.* [2]. The resistivity ($\rho(T)$) above T_C for manganites is found to be in an activated form described by the equation [2],

$$\rho(T > T_C) = \rho_0 \exp\left(\frac{E_a}{k_B T}\right). \quad (1)$$

E_a is the activation energy, ρ_0 and k_B denote the residual resistivity at $T \gg E_a$ and Boltzmann constant respectively. In the FM phase, the influence of $M(T)/M_{4.2}$ is more pronounced than the electron-phonon (e - ph) contribution where the latter requires an overwhelmingly large coupling constant [2]. Note that $M_{4.2}$ is the magnitude of magnetization at 4.2 K. Therefore, Mahendiran *et al.* have suggested that conventional mechanism namely, e -

ph scattering has to be put aside so as to explain the $\rho(T)$ for manganites below T_C . On the contrary, $\rho(T)$ with e - ph involvement for DMS in the paramagnetic phase is given by [1]

$$\rho(T > T_C) = \frac{C_1 + C_2 [\exp(\Theta_D/T) - 1]^{-1}}{k_B T \ln[1 + \exp((E_m - E_f)/k_B T)]}. \quad (2)$$

The term, $C_2/[\exp(\Theta_D/T) - 1]$ takes care of the e - ph contribution. Θ_D , E_f , E_m , C_1 and C_2 represent the Debye temperature, Fermi level, mobility edge and numerical constants respectively. The $\rho(T)$ in the FM phase based on the spin disorder scattering as derived by Tinbergen-Dekker is given by [3]

$$\begin{aligned} \rho_{SD}(T < T_C) &= \frac{(m_{e,h}^*)^{5/2} N (2E_F)^{1/2}}{\pi(n,p) e^2 \hbar^4} J_{ex}^2 \\ &\times \left[S(S+1) - S^2 \left(\frac{M_{TD}(T)}{M_{4.2}} \right)^2 \right. \\ &\left. - S \left(\frac{M_{TD}(T)}{M_{4.2}} \right) \tanh \left(\frac{3T_C M_{TD}(T)}{2TS(S+1)M_{4.2}} \right) \right]. \quad (3) \end{aligned}$$

N is the concentration of nearest neighbor ions (Mn's concentration) while (n,p) is the concentration of charge carriers (electrons or holes respectively). $m_{e,h}^*$ denotes effective mass of electrons or holes, $\hbar = h/2\pi$, h = Planck constant. e is the charge of an electron, E_F and J_{ex} are the Fermi and FM exchange interaction energies respectively while S is the spin quantum number. Equation (3) becomes equivalent to Kasuya [4] if one replaces the term, $\tanh[3T_C M_{TD}(T)/2TS(S+1)M_{4.2}]$ with 1. Again, an accurate equation for the $\rho(T)$ below T_C is still lacking since spin disorder scattering alone is insufficient as shown by Tinbergen and Dekker [3] as well as reviewed by Ohno [5]. Hence, it is desirable to derive a formula that could describe the transport mechanism of ferromagnets for the whole temperature range i.e., for both paramagnetic and FM phases and even at very low T . With this in

mind, the ionization energy based Fermi-Dirac statistics (iFDS) as derived in Ref. [6, 8, 9, 10, 11] and spin disorder scattering based resistivity models derived by both Tinbergen-Dekker and Kasuya will be employed in order to derive ρ as a function of T , ionization energy (E_I) and $M_\rho(T, M_{4.2})$. The consequences of $\rho(T, E_I, M_\rho(T, M_{4.2}))$ that arises from the variation of T , E_I and $M_\rho(T, M_{4.2})$ are discussed in detail based on the experimental data reported by Van Esch *et al.* [1] and Mahendiran *et al.* [2].

2. RESISTIVITY MODEL

The total current in semiconducting ferromagnets with contributions from both paramagnetic and FM phases is $J = \sum_\nu J_\nu$, $\nu = e^\downarrow, se^\uparrow, h^\downarrow, sh^\uparrow$. For convenience, the spin-up, \uparrow denotes the direction of the magnetic field or a particular direction below T_C , while the spin-down, \downarrow represents any other directions. Note that the total energy (Kinetic + Magnetic), $E_{K+M}^\uparrow \neq E_{K+M}^\downarrow$ due to energy level splitting below T_C . As such, the total current can be simplified as $J = J_e^\downarrow + J_{se}^\uparrow = J_e + J_{se}$ if the considered system is a n -type while $J = J_h + J_{sh}$ if it is a p -type. J_e and J_h are the spin independent charge current (electrons and holes respectively) in the paramagnetic phase whereas J_{se} and J_{sh} are the spin-assisted charge current in the FM phase. Thus the total resistivity (n or p -type) can be written as

$$\begin{aligned} \rho^{-1} &= \rho_{e,h}^{-1} + \rho_{se,sh}^{-1} \\ &= \left[\frac{m_{e,h}^*}{(n,p)e^2\tau_e} \right]^{-1} + \left[\frac{m_{e,h}^*}{(n,p)e^2\tau_{SD}} \right]^{-1}. \end{aligned} \quad (4)$$

τ_{SD} represents the spin disorder scattering rate. The carrier density for the electrons and holes (n, p) based on iFDS are given by [6, 8, 9, 10, 11]

$$n = 2 \left[\frac{k_B T}{2\pi\hbar^2} \right]^{3/2} (m_e^*)^{3/2} \exp \left[\frac{E_F - E_I}{k_B T} \right]. \quad (5)$$

$$p = 2 \left[\frac{k_B T}{2\pi\hbar^2} \right]^{3/2} (m_h^*)^{3/2} \exp \left[\frac{-E_F - E_I}{k_B T} \right]. \quad (6)$$

The derivation of iFDS, $f(E_I) = \exp[-\mu - \lambda(E_{initial\ state} \pm E_I)]$ by employing the restrictive conditions, $\sum_i^\infty dn_i = 0$ and $\sum_i^\infty (E_{initial\ state} \pm E_I)_i dn_i = 0$ is well documented (including its applications) in the Refs. [6, 7, 8, 9, 10, 11, 12, 13]. $E_{initial\ state}$ denotes the energy at certain initial state and the Lagrange multipliers, $\mu_e + \lambda E_I = -\ln[(n/V)(2\pi\lambda\hbar^2/m_e)^{3/2}]$, $\mu_h - \lambda E_I = \ln[(p/V)(2\pi\lambda\hbar^2/m_h)^{3/2}]$ and $\lambda = 1/k_B T$. V is the volume in \mathbf{k} space and the gap-parameter, E_I that represents electron-ion attraction is also a parameter that

measures the combination of electrons and its strain field due to neighboring ions, which is nothing but polarons [6, 14]. The absolute value of E_I can be obtained from [6], $E_I = e^2/8\pi\epsilon\epsilon_0 r_B$. ϵ and ϵ_0 are the dielectric constant and permittivity of free space respectively, r_B is the Bohr radius. Furthermore, the variation of E_I with magnetic field, \mathbf{H} will give rise to an inverse variation on r_B that also takes care of the polaronic effect [6, 14]. Substituting $1/\tau_e = AT^2$ (due to electron-electron interaction), Eqs. (3) and (5) or (6) into Eq. (4), then one can arrive at

$$\rho_{e,se}(T) = \frac{AB \exp[(E_I + E_F)/k_B T]}{AT^{3/2}[M_\rho(T, M_{4.2})]^{-1} + BT^{-1/2}}. \quad (7)$$

In which, $A = [A_{e,h}/2e^2(m_{e,h}^*)^{1/2}][2\pi\hbar^2/k_B]^{3/2}$, $B = 2m_{e,h}^* N(\pi E_F)^{1/2} J_{ex}^2 / e^2 \hbar k_B^{3/2}$ and $\tau_{SD}^{-1} = [N(2E_F)^{1/2}(m_{e,h}^*)^{3/2}/\pi\hbar^4] J_{ex}^2 M_\rho(T, M_{4.2})$. $A_{e,h}$ is the T independent electron-electron scattering rate constant. The empirical function of the normalized magnetization is given by

$$M_\rho(T, M_{4.2}) = 1 - \frac{M_\rho(T)}{M_{4.2}}. \quad (8)$$

Equation (8) is an empirical function that directly quantifies the influence of spin alignments in the FM phase on the transport properties of charge and spin carriers [14] in accordance with Eq. (7). In other words, the only way to obtain $\frac{M_\rho(T)}{M_{4.2}}$ is through Eq. (8). In fact, Eq. (8) is used to calculate $M_{TD}(T)/M_{4.2}$ and $M_K(T)/M_{4.2}$ by writing $S(S+1) - S^2(\frac{M_{TD}(T)}{M_{4.2}})^2 - S(\frac{M_{TD}(T)}{M_{4.2}}) \tanh[\frac{3T_C M_{TD}(T)}{2TS(S+1)M_{4.2}}] = M_\rho(T, M_{4.2})$ and $S(S+1) - S^2(\frac{M_K(T)}{M_{4.2}})^2 - S(\frac{M_K(T)}{M_{4.2}}) = M_\rho(T, M_{4.2})$ respectively. Consequently, one can actually compare and analyze the $M_\alpha(T)/M_{4.2}$ ($\alpha = TD, K, \rho$) calculated from Tinbergen-Dekker (TD), Kasuya (K) and Eq. (7) with the experimentally measured $M_{exp}(T)/M_{4.2}$. However, one has to switch to Eq. (9) given below for the hole-doped strongly correlated non-ferromagnetic semiconductors, which is again based on iFDS [6, 7],

$$\rho_h = \frac{A_h(m_h^*)^{\frac{-1}{2}}}{2e^2} \left[\frac{2\pi\hbar^2}{k_B} \right]^{3/2} T^{1/2} \exp \left[\frac{E_I + E_F}{k_B T} \right]. \quad (9)$$

3. DISCUSSION

3.1. Diluted magnetic semiconductors

It is the purpose of this paper to explain the transport mechanism below T_C without violating the physical properties known in $\rho(T > T_C)$. The discussion on

the mechanism of transport properties of ferromagnets is seen through the eyes of resistivity measurements both in the presence of and in the absence of \mathbf{H} . The resistivity measurements [1] and its fittings based on Eqs. (7) and (9) are shown in Fig. 1 a) and b) respectively for $\text{Ga}_{1-x}\text{Mn}_x\text{As}$. Literally, one needs two fitting parameters (A and E_I) for $\rho(T > T_C)$ and another two (B and $M_\rho(T, M_{4.2})$) for $\rho(T < T_C)$. All the fitting parameters are given in Table I. Note that $S = 1$ and $5/2$ are employed for the fittings of $M_K(T)/M_{4.2}$ while T_C and T_{cr} were determined from the experimental resistivity curves, *not* from the magnetization measurements or any other techniques. The deviation of $M_K(T)/M_{4.2}$ from the $M_{exp}/M_{4.2}$ increases with S from $1 \rightarrow 5/2$. The $\rho(T)$ is found to increase with x from 0.060 to 0.070 due to the mechanism proposed by Van Esch *et al.* [1, 15] and Ando *et al.* [16]. They proposed that neutral Mn^{3+} acceptors that contribute to magnetic properties could be compensated by As, where for a higher concentration of Mn, instead of replacing Ga it will form a six-fold coordinated centers with As (Mn^{6As}) [1, 15, 16]. These centers will eventually reduce the magnitude of ferromagnetism (FM) in DMS due to the loss of spin-spin interaction between $\text{Mn}(3d^5)$ and h . Parallel to this, Mn^{6As} formation is substantial in such a way that Mn^{3+} ions do not substitute Ga^{3+} ions. Therefore, $\rho(T)$ will be influenced by Mn^{6As} clusters, defects and Ga-Mn-As phase simultaneously significantly in this range of x . This is also indeed in fact in accordance with iFDS based resistivity models since if one assumes Mn^{2+} ($E_I = 1113 \text{ kJmol}^{-1}$) or Mn^{3+} ($E_I = 1825 \text{ kJmol}^{-1}$) substitutes Ga^{3+} ($E_I = 1840 \text{ kJmol}^{-1}$), then $\rho(T)$ should further decrease [6] with x , which is not the case here. Thus, iFDS also suggests that Mn^{2+} or Mn^{3+} do not substitute Ga^{3+} . Interestingly, the T_{cr} s observed in $\text{Ga}_{0.940}\text{Mn}_{0.060}\text{As}$ ($T_{cr} = 10 \text{ K}$, annealed: 370°C) and $\text{Ga}_{0.930}\text{Mn}_{0.070}\text{As}$ ($T_{cr} = 12 \text{ K}$, as grown) are identical with the calculated values, where $E_I + E_F = 8 \text{ K}$ and 12 K respectively. $E_I + E_F$ is actually equivalent to T_{cr} because of its exponential contribution as shown in Eq. (7). The calculated carrier density using $E_I + E_F$ (8, 12 K), $m_h^* = \text{rest mass}$ and Eq. (6) is $2.4 \times 10^{19} \text{ cm}^{-3}$. Below T_C , spin alignments enhance the contribution from J_{se} and reduces the exponential increase of $\rho(T)$. This reduction in $\rho(T)$ is as a result of dominating J_{se} and small magnitude of $E_I + E_F$ (8-12 K), consequently its effect only comes around at low T as clearly shown in Fig. 1 a). The $\text{Ga}_{0.930}\text{Mn}_{0.070}\text{As}$ samples after annealing at 370°C and 390°C do not indicate any FM [1] (Fig. 1 b)). Thus the fittings are carried out with Eq. (9) that only require two parameters namely, A and $E_I + E_F$ since $J_{se} = 0$ (there is no observable T_C) and/or $dM_\alpha(T)/M_{4.2}dT = 0$ ($M_\rho(T, M_{4.2}) = \text{constant}$). The exponential increase of $\rho(T)$ is due to $E_I + E_F$ as given in Eq. (9) with zilch J_{se} contribution.

Figure 1 c) and d) indicate the calculated normalized magnetization, $M_\alpha(T)/M_{4.2}$ obtained from Eq. (7). Note

that $M_{\rho,TD,K}(T)/M_{4.2}$ is a fitting parameter that has been varied accordingly to fit $\rho(T < T_C)$. As a matter of fact, $M_\rho(T, M_{4.2})$ is used to calculate $M_{\rho,TD,K}(T)/M_{4.2}$ with $S = 1$. $M_{\rho,TD,K}(T)/M_{4.2}$ is also compared with the experimentally determined [1] $M_{exp}(T)/M_{4.2}$ as depicted in Fig. 1 d). One can easily notice the relation, $M_{TD}(T)/M_{4.2} > M_K(T)/M_{4.2} > M_\rho(T)/M_{4.2} > M_{exp}(T)/M_{4.2}$ from Fig. 1 c) and d). As such, $M_\rho(T)/M_{4.2}$ determined from Eq. (7) is the best fit for the experimentally measured $M_{exp}(T)/M_{4.2}$. Obviously, the higher number of aligned spins as calculated from Eq. (7) using $M_\rho(T)/M_{4.2}$ compared to $M_{exp}(T)/M_{4.2}$ is due to the ability of both J_e and J_{se} to follow the easiest path. Simply put, resistivity measures only the path with relatively lowest E_I and with easily aligned spins that complies with the principle of least action. In contrast, magnetization measurement quantifies the average of all the spins' alignments. On the other hand, the discrepancies of $M_{TD}(T)/M_{4.2}$ with $M_{exp}(T)/M_{4.2}$ and $M_K(T)/M_{4.2}$ with $M_{exp}(T)/M_{4.2}$ are due to long range FM hole-hole and AFM Mn-hole interactions [1] apart from the ability of both J_e and J_{se} to follow the easiest path. The violation between $M_{TD,K}(T)/M_{4.2}$ and $M_{exp}(T)/M_{4.2}$ suggests that the spin disorder scattering alone is inadequate, in which, the principle of least action have had played an enormous role.

3.2. Manganites

Now switching to manganites, Mahendiran *et al.* [2] discussed $\rho(T < T_C)$ with respect to Eq. (1) and obtained the activation energy, $E_a = 0.16 \text{ eV}$ for $x = 0.1$ and 0.2 of $\text{La}_{1-x}\text{Ca}_x\text{MnO}_3$ samples at 0 T . Using Eq. (7) however, $E_I + E_F$ for the former and latter samples are calculated to be 0.12 and 0.11 eV respectively. The calculated carrier density using $E_I + E_F$ ($0.12, 0.11 \text{ eV}$), $m_h^* = \text{rest mass}$ and Eq. (6) is approximately 10^{17} cm^{-3} . In the presence of $\mathbf{H} = 6 \text{ T}$, $E_I + E_F$ is computed as 0.0776 eV for $x = 0.2$ that subsequently leads to $p = 10^{18} \text{ cm}^{-3}$. It is proposed that the activated behavior for $\rho(T > T_C)$ is due to E_I , Coulomb interaction between ion and electron or rather due to the polaronic effect [6, 10]. The fittings are shown in Fig. 2 a) and b) while its fitting parameters are listed in Table I. Theoretically [6, 10], Ca^{2+} ($E_I = 868 \text{ kJmol}^{-1}$) $<$ La^{3+} ($E_I = 1152 \text{ kJmol}^{-1}$), therefore $\rho(T)$ is expected to decrease with Ca^{2+} doping significantly. Contradicting to that, only a small difference of $E_I + E_F$ between $x = 0.1$ (0.12 eV) and 0.2 (0.11 eV) is observed due to Mn^{4+} 's compensation effect where the quantity of Mn^{4+} increased 6% from $x = 0.1$ (19%) to 0.2 (25%) [2]. To clearly see this, the difference of E_I between Ca^{2+} and La^{3+} is calculated, which is $1152 - 868 = 284 \text{ kJmol}^{-1}$ and subsequently it is compared with the 6% increment of $\text{Mn}^{3+ \rightarrow 4+}$ ($E_I = 4940 \text{ kJmol}^{-1}$), which is $0.81(1825) + 0.19(4940) - 0.75(1825) - 0.25(4940) =$

187 kJmol⁻¹. Consequently, the actual difference is only 284 - 187 = 97 kJmol⁻¹ instead of 284 kJmol⁻¹. This simple calculation exposes that Ca²⁺'s contribution has been compensated with 6% additional Mn⁴⁺. All the values of E_I discussed above were averaged in accordance with $E_I[X^{z+}] = \sum_{i=1}^z \frac{E_{Ii}}{z}$ and should not be taken literally since those E_I s are not absolute values. The absolute values need to be obtained from the r_B dependent E_I equation stated earlier. Prior to averaging, the 1st, 2nd, 3rd and 4th ionization energies for all the elements mentioned above were taken from Ref. [18].

As is well known, at 6 T, La_{0.8}Ca_{0.2}MnO₃ indicate a much lower resistivity (Fig. 2 b)). The result that larger **H** giving rise to conductivity at $T > T_C$ is due to relatively large amount of aligned spins at higher T or **H** gives rise to J_{se} at a higher T . Hence, T_C at 6 T $> T_C$ at 0 T and one can also conclude, r_B (at 6 T) $> r_B$ (at 0 T) due to the inequality, $E_I + E_F = 78$ meV (at 6 T) $< E_I + E_F = 112$ meV (at 0 T) complying with Eq. (7) and iFDS. Figure 2 c) and d) depict calculated $M_\alpha(T)/M_{4.2}$ with $S = 1$ and $M_{exp}(T)/M_{4.2}$ for $x = 0.2$. Calculated $M_{TD}(T)/M_{4.2}$ is dropped for La_{1-x}Ca_xMnO₃ since $M_K(T)/M_{4.2}$ seems to be a better approximation than $M_{TD}(T)/M_{4.2}$ as indicated in Fig. 1 c) and d). Millis *et al.* [17] have shown theoretically that double exchange mechanism (DEM) alone is inadequate and one needs to incorporate polaronic effect into DEM. In fact, Eq. (7) takes both polaronic effect (E_I) and DEM ($M_\alpha(T)/M_{4.2}$) into account and yet there is a discrepancy between $M_\rho(T)/M_{4.2}$ and $M_{exp}(T)/M_{4.2}$ though Eq. (7) reproduces $\rho(T)$ at all T range accurately. Again, this incompatibility is due to the principle of least action as stated earlier. Note that the discrepancy between $M_K(T)/M_{4.2}$ and $M_\rho(T)/M_{4.2}$ indicate the inadequacy pointed out by Millis *et al.* [17], not the former. This inadequacy may not be clear from Fig. 2 d) because the deviation is large with respect to magnetization in a narrow range of T (careful observation will reveal this though). In addition, the manganites' charge transport mechanism below T_C is also in accordance with Eq. (7) because the term, $M_\rho(T, M_{4.2})$ handles the exchange interactions' complexities separately for DMS and manganites. For example, one can clearly notice the different type of discrepancies between DMS and manganites by comparing the empirical function, $M_\alpha(T)/M_{4.2}$ ($\alpha = \rho$, exp) between Fig. 1 d) and Fig. 2 d). Hence, Eq. (7) is suitable for both types of ferromagnets, be it diluted or concentrated. In conclusion, the resistivity model that have incorporated the polaronic and magnetization effects has been derived based on iFDS and spin disorder scattering theories. This model is able to explain the transport mechanism below the Curie temperature without violating the physical properties above T_C . The discrepancy of the magnetization curves calculated from this resistivity model with the experimental data of DMS arises as a result of the ability of both spin and charge

TABLE I: Calculated values of T independent electron-electron scattering rate constant (A), B , which is a function of T independent spin disorder scattering rate constant and spin exchange energy (J_{ex}) as well as the ionization energy (E_I). Note that T_C and T_{cr} were obtained from the resistivity curves. All these parameters are for Mn doped Ga_{1-x}Mn_xAs (as grown and annealed at 370 °C, 390 °C) and Ca doped La_{1-x}Ca_xMnO₃ (measured at 0 and 6 T) systems. All Ga_{1-x}Mn_xAs samples were measured at 0 T.

FIG. 1: Equation (7) has been employed to fit the experimental $\rho(T)$ plots for Ga_{1-x}Mn_xAs as given in a) whereas Eq. (9) is used to fit the plots in b). All fittings are indicated with solid lines. b) is actually for annealed non-ferromagnetic Ga_{0.930}Mn_{0.070}As samples. c) and d) show the T variation of calculated $M_\alpha(T)/M_{4.2}$ ($\alpha = K, TD, \rho$) with $S = 1$ for $x = 0.060$ and 0.070 respectively. $M_K(T)/M_{4.2}$ is also calculated with $S = 5/2$ to indicate the type of deviation one should expect with increasing S . The experimental $M_{exp}(T)/M_{4.2}$ plots is only available for $x = 0.070$ (as grown) as shown in d).

currents to follow the easiest path according to the principle of least action, long range ferromagnetic and short range antiferromagnetic interactions. Whereas for manganites, this discrepancy is still noticeable solely because of the principle of least action.

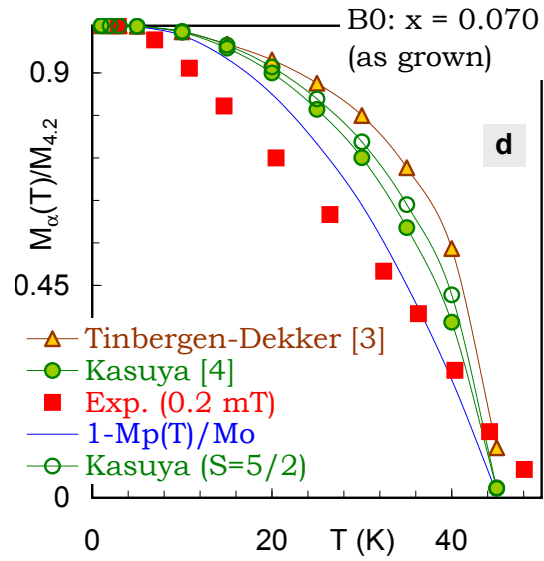
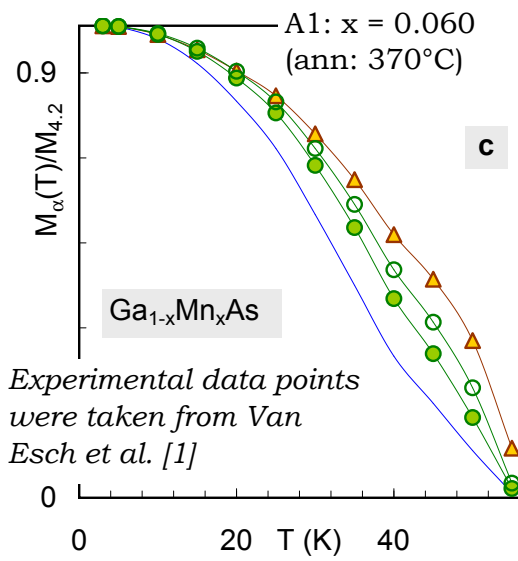
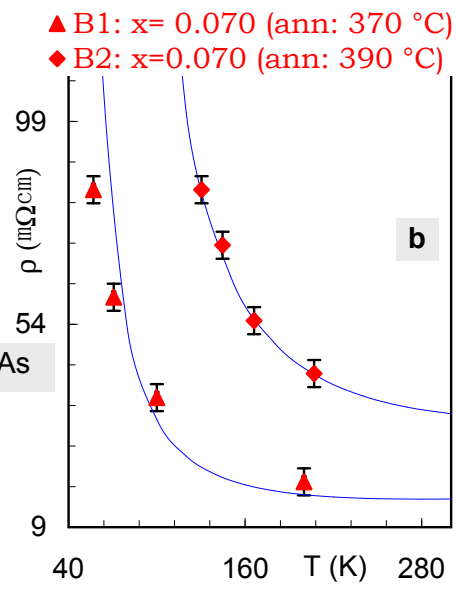
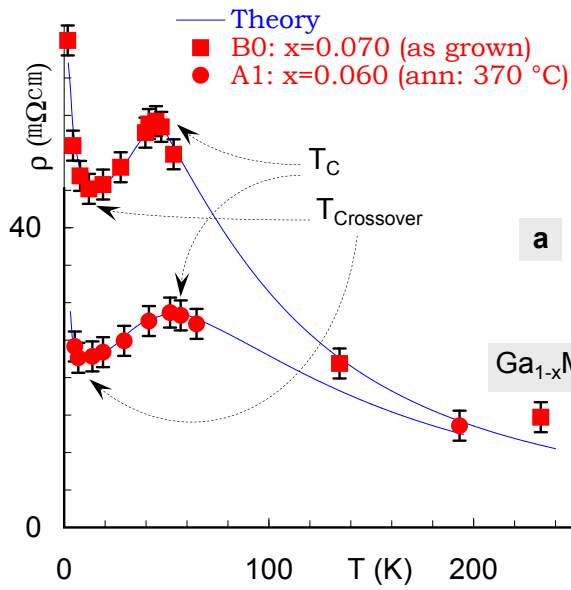
Acknowledgments

The author is grateful to Arulsamy Innasimuthu, Sebastianmammal Innasimuthu, Arokia Das Anthony and Cecily Arokiam of CMG-A for their financial assistances. ADA also thanks Bryne J.-Y. Tan, Jasper L. S. Loverio and Hendry Izaac Elim for their kind help with the extraction of experimental data points as given in Figure 1a) and 1b) as well as for providing some of the references. ADA thanks Prof. Feng Yuan Ping for his support to participate in ICMAT-2003, Singapore.

-
- [1] A. Van Esch, L. Van Bockstal, J. De Boeck, G. Verbanck, A. S. van Steenberghe, P. J. Wellmann, B. Grietens, R. Bogaerts, F. Herlach, G. Borghs, Phys. Rev. B 56 (1997) 13103.

FIG. 2: Experimental plots of $\rho(T)$ for La_{1-x}Ca_xMnO₃ at $x = 0.1, 0.2$ and 0.2 (6 T) have been fitted with Eq. (6) as depicted in a) and b). All fittings are indicated with solid lines. Whereas c) and d) show the T variation of calculated $M_\alpha(T)/M_{4.2}$ ($\alpha = K, \rho$) with $S = 1$ for $x = 0.1$ and 0.2 respectively. The experimental $M_{exp}(T)/M_{4.2}$ plots is only available for $x = 0.2$, which is given in d).

- [2] R. Mahendiran, S. K. Tiwary, A. K. Raychaudhuri, T. V. Ramakrishnan, R. Mahesh, N. Rangavittal, C. N. R. Rao, Phys. Rev. B 53 (1996) 3348.
- [3] Tineke Van Peski-Tinbergen, A. J. Dekker, Physica 29 (1963) 917.
- [4] T. Kasuya, Prog. Theor. Phys. 16 (1956) 58.
- [5] H. Ohno, Science 281 (1998) 951.
- [6] A. Das Arulsamy, cond-mat/0212202 (<http://arxiv.org>).
- [7] A. Das Arulsamy, cond-mat/0408115 (<http://arxiv.org>).
- [8] A. Das Arulsamy, Physica C 356 (2001) 62.
- [9] A. Das Arulsamy, Phys. Lett. A 300 (2002) 691.
- [10] A. Das Arulsamy, in *Superconductivity research at the leading edge*, edited by Paul S. Lewis (Nova Science Publishers, New York, 2004) pp. 45-57.
- [11] A. Das Arulsamy, P. C. Ong, M. T. Ong, Physica B 325 (2003) 164.
- [12] A. Das Arulsamy, Physica B (in press).
- [13] A. Das Arulsamy, cond-mat/0206293 (<http://arxiv.org>).
- [14] A. Das Arulsamy, cond-mat/0406030 (<http://arxiv.org>).
- [15] L. Van Bockstal, A. Van Esch, R. Bogaerts, F. Herlach, A. S. van Steenbergen, J. De Boeck, G. Borghs, Physica B 246-247 (1998) 258.
- [16] K. Ando, T. Hayashi, M. Tanaka, A. Twardowski, J. Appl. Phys. 53 (1998) 6548.
- [17] A. J. Millis, P. B. Littlewood, B. I. Shraiman, Phys. Rev. Lett 74 (1995) 5144.
- [18] M. J. Winter, (<http://www.webelements.com>).



Sample	Ann. $T(H)$ °C(Tesla)	A [Calc.]	B [Calc.]	$E_I + E_F$ [Calc.] K(meV)	$T_C(T_{cr})$ K [1,2]
Ga _{0.940} Mn _{0.060} As [1]	370 (0)	4.5	400	8 (0.69)	50 (10)
Ga _{0.930} Mn _{0.070} As [1]	As grown (0)	9.2	400	12 (1.04)	45 (12)
Ga _{0.930} Mn _{0.070} As [1]	370 (0)	0.02	~	280 (24.2)	~
Ga _{0.930} Mn _{0.070} As [1]	390 (0)	0.03	~	400 (34.5)	~
La _{0.9} Ca _{0.1} MnO ₃ [2]	~ (0)	10	0.65	1400 (121)	222 (~)
La _{0.8} Ca _{0.2} MnO ₃ [2]	~ (0)	10	1.2	1300 (112)	246 (~)
La _{0.8} Ca _{0.2} MnO ₃ [2]	~ (6)	5	3.2	900 (78)	251 (~)

